CHEMISTRY OF MATERIALS

pubs.acs.org/cm

Article

Plasmonics under Attack: Protecting Copper Nanostructures from Harsh Environments

Arin S. Preston, Robert A. Hughes, Trevor B. Demille, and Svetlana Neretina*

Cite This: *Chem. Mater.* 2020, 32, 6788–6799

Read Online

ABSTRACT: The functionality of well-tailored nanomaterials can only be retained if they are robust to the environmental factors in which they operate. The inability of Cu to withstand such factors is largely responsible for its current status as a second-tier plasmonic nanomaterial. Herein, it is demonstrated that atomic layer deposition can be used as a pliable technique for the application of oxide coatings to substrate-based Cu nanostructures where suitably protected structures become robust to oxidation, high temperatures, and aqueous, acidic, and alkaline solutions without unduly influencing important plasmonic properties. Moreover, strategies are presented for maximizing plasmonic near-fields and allowing for the transport of hot electrons while maintaining coating integrity. The findings demonstrate that there does not exist a one-solution-fits-all approach but that coating design must follow an application-specific methodology. Within the scope of the investigation, alumina, hafnia, titania, and combinations thereof were all shown to be effective under certain conditions, but where hafnia shows the greatest durability in extreme pH environments and alumina-hafnia multilayers provide Cu with protection from oxidation to temperatures as high as 600 °C. The work advances the use of Cu nanostructures as durable plasmonic materials and provides broad-based strategies for protecting other vulnerable nanomaterials from harsh environments.

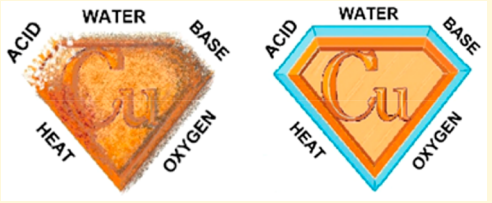

INTRODUCTION

Material stability, be it photo, thermal, chemical, mechanical, or a combination thereof, is a ubiquitous subject of fundamental importance. It often decides whether a technology is viable, reliable, and sustainable and where the outcomes have economic, environmental, and social impacts. Even though numerous applications call for low-cost earth-abundant metals that can withstand an environmental attack while retaining important physicochemical properties, it is a call that is rarely answered by elemental metals. Nevertheless, the use of these same metals is pervasive due to material solutions that mitigate environmental sensitivities. The use of Cu interconnects in electronics is, for example, a viable option only because dielectric coatings are used to passivate its otherwise reactive surface. If these same earth-abundant metals are to be exploited as nanomaterials, then it will likewise call for innovative application-based solutions, but where the challenges encountered are amplified by large surface-to-volume ratios, intricate nanostructure architectures, and heightened chemical reactivity.

Despite being prone to oxidation under ambient conditions, Cu has emerged as a standout nanomaterial with applications in catalysis,[1,2] electronics,[3] displays,[4−6] and sensing.[7−9] With Cu exhibiting a facet-dependent catalytic activity, a high electrical conductivity, and size- and shape-dependent plasmonic properties, there has been a strong impetus for formulating a colloidal chemistry that now encompasses every common nanostructure architecture.[10−17] As a plasmonic material, Cu usage lags well-behind that of Au and Ag. Putting aside environmental sensitivities, there is a strong case to be made for Cu as a material of choice for low-cost plasmonics. Current Au and Ag prices are 9600 and 100 times that of Cu, respectively. Although Cu plasmons are strongly damped when photon energies exceed its interband transition value of 2.1 eV,[16] the localized surface plasmon resonance peak (LSPR) is comparable to that of Au in a low loss window extending from 620 to 750 nm.[8,11,18] Interestingly, Zheng et al.[11] have recently shown that specific plasmon modes of Cu nanocubes are relatively impervious to the interband transition, displaying an intense LSPR peak centered at 585 nm (2.12 eV). The result suggests that the usable window for Cu plasmonics can be extended through rational design. Also noteworthy is that hot holes formed during the dephasing of the Cu plasmon have a lifetime and energy dependence that is distinct from Au,[19,20] a property of significance to plasmonic-based photocatalysis and photovoltaics. With alternate plasmonic materials[21,22] showing lower LSPR quality factors[22,23] or requiring cost-prohibitive epitaxial growth modes,[21] Cu remains unique among these nanomaterials. Nevertheless, Cu has, to a large extent, been abandoned by the device community as a candidate material

Received: June 27, 2020
Revised: July 9, 2020
Published: July 10, 2020

https://dx.doi.org/10.1021/acs.chemmater.0c02715
Chem. Mater. 2020, 32, 6788–6799

for on-chip plasmonics due to its inability to withstand environmental factors.

The applications for plasmonic materials are so diverse that they collectively place a set of demands on materials so stringent that there exists no single material that can meet all of them. With the ability to confine light energy into subwavelength volumes, plasmonic nanostructures by their very nature create an energy intense environment that generates electric fields, hot electrons, and heat which, by themselves, can lead to morphological and chemical disruptions, especially when illuminated with high-intensity light sources such as lasers or concentrated solar.[24,25] To meet the demands of sensing technologies, plasmonic nanostructures must sustain performance in air, H_2O (liquid, vapor, and steam), acids, bases, solvents, reactive gases (e.g., CO, H_2, SO_2), and a wide range of chemical and biological analytes. Applications requiring elevated temperatures, such as those associated with refractory plasmonics[25,26] or catalysis,[27,28] must maintain functionality in an environment conducive to diffusion-induced shape changes and heightened chemical reactivity. With such demands, it is not surprising that Cu has been underutilized as a plasmonic material because its nanostructures readily oxidize under ambient conditions, leach in aqueous environments, show poor corrosion resistance, and, like all noble metals, lack dimensional stability at elevated temperatures.

The drawbacks associated with Cu largely preclude its use in on-chip plasmonic devices unless protective coatings are applied. This limits its usage to applications where plasmonic properties are not unduly influenced or negated by the coating. Oxides are the most obvious candidate materials for protective coatings in that they can (i) transmit light, (ii) offer extremely low oxygen self-diffusion coefficients, (iii) choke off metal surface diffusion pathways, and (iv) provide a high resistance to corrosive environments. There also exists a set of important sensing techniques where the encapsulation of plasmonic nanostructures within pinhole-free oxide shells is carried out, not merely to protect a vulnerable metal but as a means to enhance device performance. Shell-isolated nanoparticle-enhanced Raman spectroscopy (SHINERS)[29−32] is a sensing technique that is analogous to surface-enhanced Raman scattering (SERS),[32] but where the separation of the analyte from the plasmonic metal by a thin chemically inert dielectric spacer allows for sensing modalities that (i) are often more reproducible than SERS, (ii) allow for detection in corrosive environments and at elevated temperatures, (iii) isolate the metal surface from application-specific environmental contaminants, (iv) create a noninvasive environment for biological species that are sensitive to nanometal surfaces or leached metal ions, and (v) result in a sensing surface with improved recyclability. Similarly, shell-isolated nanoparticle enhanced fluorescence (SHINEF)[33−35] utilizes plasmonic near-fields to enhance the fluorescence of an adjacent fluorophore, but where a spacer is required to prevent the quenching of the fluorescence by the metal. Additionally, dual-mode SHINERS−SHINEF detection is an emerging technique with biomedical applications.[33]

The use of coatings in on-chip plasmonic applications is becoming increasingly prevalent. Aluminum has, notably, emerged as a material of significance for ultraviolet plasmonics[36,37] ostensibly due to a naturally occurring protective oxide layer that provides air stability to an otherwise highly reactive element. The application of synthetic coatings as physical and chemical barriers to substrate-based Ag structures[38−45] is now receiving considerable attention, a trend that is partially due to the poor shelf life of Ag-based devices. Albrecht et al.[46] advanced the use of Au in refractory plasmonic applications by demonstrating that lithographically defined Au nanorods, when coated with a thin layer of Al_2O_3, can retain their shape when heated to temperatures as high as 800 °C. In a subsequent report,[39] they showed that the same strategy could be successfully applied to numerous other metals, but where the results for Cu proved disappointing. Li et al.[47] demonstrated that graphene, when applied to Cu nanostructures formed through solid-state dewetting, slowed the rate of oxidation under ambient conditions. Duan et al.[48] have demonstrated the utility of embedding electrochemically synthesized Cu nanowires in a polycarbonate template.

Even though protective coatings for on-chip plasmonics have been advanced, there has not yet been a comprehensive effort directed toward the design of durable application-specific coatings where the coating is engineered to protect the underlying nanostructure from particular environmental threats or that accentuate critical plasmonic properties. Herein, we demonstrate atomic layer deposition (ALD)[38,49] as a viable method for applying oxide coatings to substrate-based Cu nanostructures in a manner that effectively mitigates environmental sensitivities while preserving important plasmonic properties. Endurance testing reveals that suitably designed coatings can protect Cu against oxidation, high temperatures, and aqueous, acidic, and alkaline solutions, but where no single coating material is able to withstand all environmental factors. The results advance the use of Cu as an attractive low-cost nanomaterial for on-chip plasmonic devices while emphasizing the importance of trade-offs in terms of attaining durability−performance characteristics that meet the needs of specific applications.

RESULTS AND DISCUSSION

The results presented in this section describe the processing science that was formulated to obtain substrate-supported Cu nanostructures that are encapsulated within an ultrathin pinhole-free oxide shell as well as an assessment of their durability when exposed to harsh environments. The Cu nanostructures used were either substrate-truncated spheres or cuboctahedra where the latter was used to assess the impact of faceting on shell formation and durability. The substrate-truncated spheres were produced as both periodic arrays with a narrow size distribution and as structures with randomized size and placement. Both formats proved effective in durability studies, but where the arrayed structures presented a superior platform for cases where a statistical analysis of nanostructure failure rates is desired. Al_2O_3 (alumina), HfO_2 (hafnia), and TiO_2 (titania) were assessed as coatings because they have favorable refractory and corrosion-resistant properties as bulk materials and are readily deposited using the ALD technique. The coating integrity was assessed under various environmental conditions where in all cases bare Cu nanostructures were exposed to the same environment to establish baseline performance metrics. Coating failure modes are identified, and when possible, mitigation strategies are advanced.

Synthesis and Characterization of Cu Nanostructures with Oxide Coatings. Substrate-based Cu nanostructures have previously been prepared using a number of techniques including the (i) lithographic patterning of polycrystalline films,[18,39,50] (ii) dispersal and self-assembly of colloids on

https://dx.doi.org/10.1021/acs.chemmater.0c02715
Chem. Mater. 2020, 32, 6788−6799

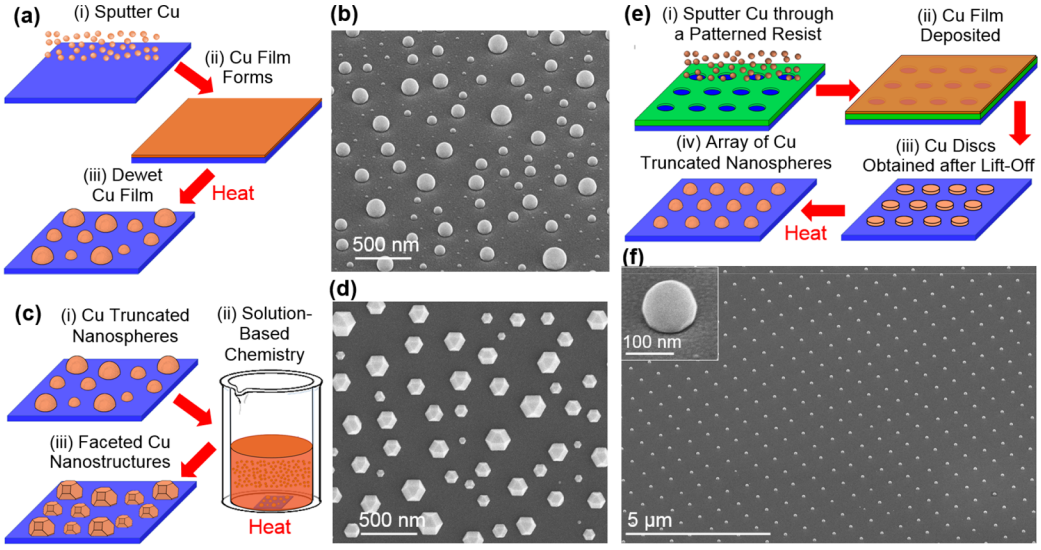

Figure 1. Scheme schematics and SEM images for substrate-based Cu nanostructures fabricated using (a,b) solid-state dewetting, (c,d) solid-state dewetting followed by a liquid-phase chemical synthesis, and (e,f) templated-dewetting facilitated by nanoimprint lithography.

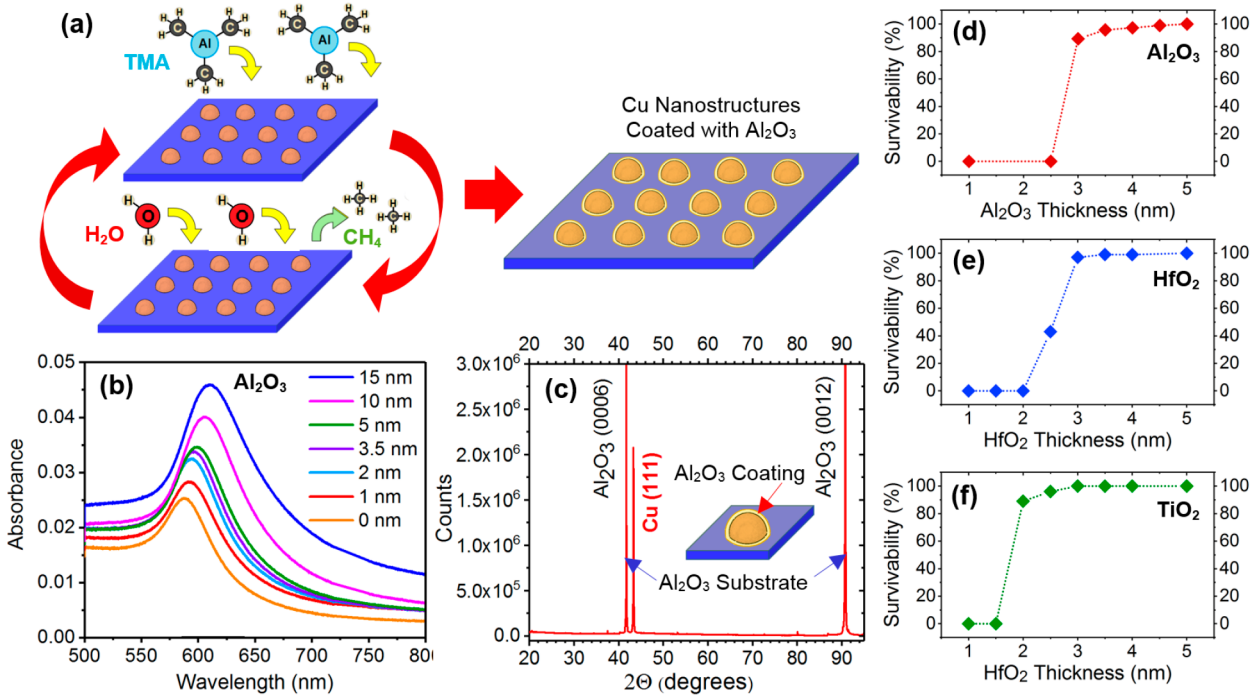

Figure 2. (a) Schematic of the cyclic ALD process used to deposit Al_2O_3 coatings on Cu nanostructures. (b) Absorbance spectra of a periodic array of 120 nm diameter Cu nanostructures for Al_2O_3 coating thicknesses ranging from 0 to 15 nm. (c) XRD data for Cu nanostructures with a 5 nm thick Al_2O_3 coating. Percent survivability of coated Cu nanostructures when exposed to nitric acid as a function of coating thickness for (d) Al_2O_3, (e) HfO_2, and (f) TiO_2.

surfaces,[12,16,51] and (iii) solid-state dewetting of films.[47,52−55] Figure 1 shows schematic representations of the three different schemes used to form Cu nanostructures in the current study as well as SEM images of the structures obtained. The first method relies on the solid-state dewetting[56] of an ultrathin sputter-deposited Cu film, a technique in which a heated film breaks up into nanoscale islands that then agglomerate so as to reduce the overall surface energy (Figure 1a). The structures realized are highly crystalline[52] with a truncated nanosphere morphology (Figure 1b). The second method, which yields highly faceted cuboctahedra, subjects the dewetted structures formed using the first method to a liquid-phase chemical synthesis that promotes facet growth (Figure 1c).[57,58] The structures obtained exhibit crisp faceting characterized by prominent {100} and {111} facets (Figure 1d). The third method, referred to as templated dewetting,[59] uses nanoimprint lithography to define a periodic array of polycrystalline Cu discs that each agglomerates into a single-crystal truncated nanosphere when subjected to high temperatures (Figure 1e).[60] The so-formed structures (Figure 1f) have a roundish morphology and narrow size distribution centered on a diameter of approximately 120 nm (Figure S1). It should be noted that all of the dewetting procedures are carried out under a H_2−Ar atmosphere to prevent the oxidation of Cu.

https://dx.doi.org/10.1021/acs.chemmater.0c02715
Chem. Mater. 2020, 32, 6788−6799

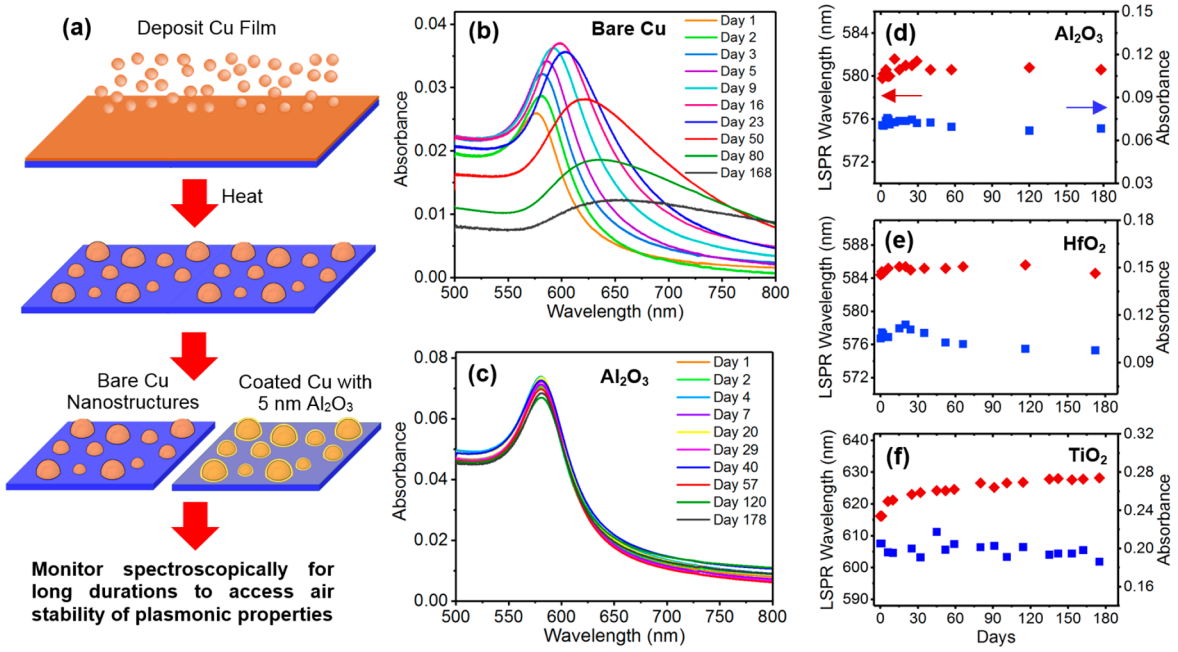

Figure 3. (a) Schematic of the procedure used to assess the air stability of coated and bare Cu nanostructures. The time dependent absorbance spectra obtained for (b) bare Cu nanostructures and (c) identical structures coated with 5 nm of Al_2O_3. Plots showing the time dependence of the LSPR wavelength (red) and maximum absorbance (blue) for Cu nanostructures coated with 5 nm of (d) Al_2O_3, (e) HfO_2, and (f) TiO_2.

Cu nanostructures produced using the various schemes were encapsulated in an oxide coating using ALD where the deposition parameters are comparable to those typically used for Al_2O_3,[61−63] HfO_2,[64,65] and TiO_2.[66,67] ALD, which has evolved into a mainstream deposition technique for the microelectronics industry, is ideally suited for the application of protective coatings to substrate-supported nanomaterials that exhibit chemical and thermal fragility. Its advantage stems from the ability to apply compositionally uniform conformal layers to intricately shaped three-dimensional objects at low temperatures where the layer thickness can be controlled with atomic-scale precision. Figure 2a shows a schematic of the ALD process for the fabrication of Al_2O_3 coatings. The deposition proceeds by sequentially exposing a surface to two chemically distinct gaseous precursors in a pulsed, alternating, and nonoverlapping manner where each pulse leads to a self-limiting "half-reaction" with the exposed surface that results in the deposition of a monolayer. A conformal film of the desired thickness can, hence, be deposited though the cyclic application of the two precursors where the number of cycles is set to the required number of monolayers. For the case of Al_2O_3, the trimethylaluminum (TMA) precursor attaches to the surface as a monolayer where its subsequent exposure to H_2O vapor leads to the oxidation of aluminum with methane (CH_4) as the byproduct. HfO_2 and TiO_2 coatings are produced in much the same manner, but where TEMAH (tetrakis(ethylmethylamido)hafnium) and TDMAT (tetrakis-(dimethylamido)titanium) are used as the source for Hf and Ti, respectively. For all cases, the as-deposited coatings are amorphous where the exact stoichiometry is ill-defined as is typical for ALD processing.

Cu nanostructures coated with ALD-deposited oxide layers were characterized to (i) determine the influence of the coating on plasmonic properties, (ii) assess whether Cu nanostructures oxidize during the coating procedure, and (iii) establish the minimum coating thickness that is free of pinholes. Figure 2b shows the absorbance spectra obtained as the thickness of the applied Al_2O_3 coating is systematically varied from 0 to 15 nm. The results reveal that the Cu LSPR is not adversely affected by the Al_2O_3 layer but instead steadily red shifts as its absorbance increases. Both of these effects are as expected because the refractive index of Al_2O_3 (n = 1.65)[62] causes a red shift in the LSPR that in turn intensifies the plasmon peak since a shift away from the Cu interband transition lessens the degree to which the LSPR is damped.[18] Similar dependencies are observed for the other oxide coatings, but where the red shift for a given thickness is greater due to the larger refractive indices of HfO_2 (n = 1.98)[68] and TiO_2 (n = 2.2)[69] (Figure S2). X-ray diffraction (XRD) measurements (Figure 2c) show the expected (111) Cu reflection with no discernible peaks originating from Cu_2O or CuO. The absence of significant Cu oxidation is corroborated by discrete dipole approximation (DDA) simulations[70] of the absorbance spectra (Figure S3). These simulations can account for the observed shift in the plasmon resonance as the Al_2O_3 coating is added without the inclusion of a Cu_2O layer. It should be noted that such a layer would lead to a substantial red shift in the plasmon resonance.[17] With pinholes in the ALD-deposited layer being highly undesirable, a statistical analysis was carried out to determine the minimum coating thickness where the vast majority of Cu nanostructures is encapsulated in their entirety. The data was obtained by exposing the structures to 1 M nitric acid for 20 min so that any pinholes would lead to the formation of an oxide shell devoid of Cu. The hollowed-out shells are readily identified in SEM images (Figure S4), and as such, provide an easily obtained metric for establishing whether a nanostructure coating has pinholes. The results, presented in Figure 2d−f, indicate that Al_2O_3, HfO_2, and TiO_2 require thicknesses of at least 4.5, 4, and 3 nm to ensure shell integrity (≥98% survivability).

Durability in Air. The long-term stability of Cu nanostructures under ambient conditions was assessed for

https://dx.doi.org/10.1021/acs.chemmater.0c02715
Chem. Mater. 2020, 32, 6788−6799

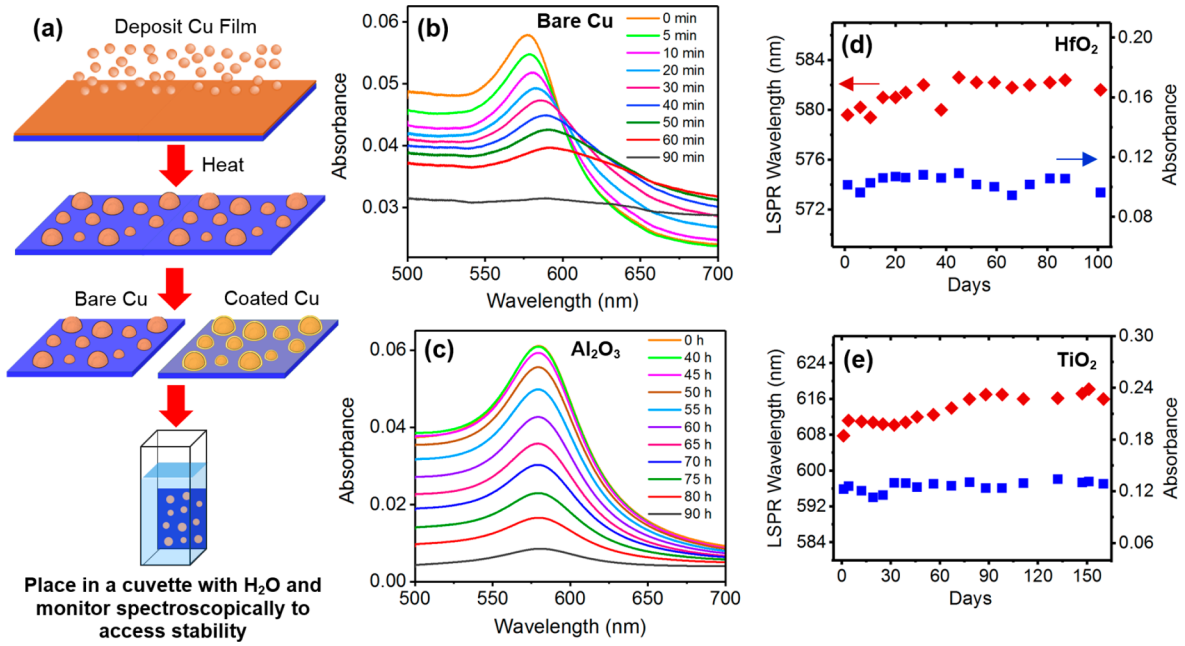

Figure 4. (a) Schematic of the procedure used to assess the H_2O stability of coated and bare Cu nanostructures. *In situ* absorbance spectra obtained for (b) bare Cu nanostructures and (c) identical structures coated with 5 nm of Al_2O_3 while continuously immersed in H_2O. Time dependence of the LSPR wavelength (red) and maximum absorbance (blue) for Cu nanostructures coated with 5 nm of (d) HfO_2 and (e) TiO_2 that were continuously immersed in H_2O except when undergoing optical characterization.

bare and oxide-coated structures. The experimental procedure, which is shown schematically in Figure 3a, begins by depositing and dewetting Cu films so as to obtain four samples with near-identical absorbance spectra. Al_2O_3, HfO_2, and TiO_2 coatings with a 5 nm thickness were applied to three of the samples, while the fourth was left bare. The absorbance spectrum of each was then monitored over a period of several months to determine the effectiveness of the coating in preventing oxidation. As expected, the prolonged exposure of the bare structures to air resulted in a continuously varying LSPR that red shifts and broadens with time (Figure 3b). The LSPR absorbance increases over the first 16 days after which it gradually falls. This behavior, which is similar to that observed in prior studies,[18,71,72] is consistent with the gradual oxidation of Cu. The red shift is caused by the encapsulation of Cu with a dielectric coating (i.e., Cu_2O), while the initial rise in absorbance is due to a decline in damping as the LSPR red shifts away from the interband transition of Cu. These effects are quite analogous to those observed when Cu nanostructures are coated with Al_2O_3 (Figure 2b), but with the key difference being that the plasmonic nanostructures are being consumed through oxidation. When the Cu nanostructures are coated with the various oxides, the plasmonic properties show no signs of deterioration for durations lasting many months. Figure 3c shows the high degree of overlap in the absorbance spectra obtained for the Al_2O_3-coated sample over the period studied where the differences observed fall within the experimental uncertainty of the measurement. Plots showing the time dependence of both the wavelength and maximum absorbance of the Cu LSPR for the three coating materials show no changes of significance (Figure 3d–f), indicating that they all effectively passivate the Cu surface under atmospheric conditions. The results strongly suggest that the plasmonic properties of Cu can be retained for long durations, a property of significance to applications requiring a long shelf life.

Durability in Aqueous Media. Durability tests in aqueous media proceeded in much the same manner as those carried out in air (Figure 4a). The LSPR for samples showing long-term stability (i.e., > 4 days) were monitored by periodically removing them from the aqueous solution (8 mL) for optical characterization, while those showing poor stability were measured *in situ*. Bare Cu nanostructures exhibit remarkably poor chemical stability in aqueous environments, showing an LSPR that is completely extinguished in less than 60 min (Figure 4b). Unprotected Cu nanostructures are highly susceptible to oxidative etching in H_2O[73] and, as such, completely disappear from the substrate surface over time. It should be noted that such effects are highly exaggerated for these substrate-based Cu nanostructures since the total number of Cu atoms on the substrate surface (i.e., 5.8×10^{15}) is exceedingly small, being outnumbered by the amount of dissolved oxygen within the H_2O by more than 200-fold under ambient conditions. When coated with 5 nm of Al_2O_3, the Cu nanostructures show improved durability, but where the plasmon is extinguished over a 90 h time frame (Figure 4c). The failure mode is one in which the Al_2O_3 coating roughens, breaches, and eventually delaminates from the surface, as the Cu nanostructure diminishes in size due to leaching (Figure S5). The continuous decline in the LSPR absorbance without a significant peak shift is consistent with a somewhat rapid hollowing process where only a relatively small number of structures are breached at any given time. Although it has been reported that the exposure of ALD-deposited Al_2O_3 films to high temperature anneals results in enhanced chemical stability,[74,75] this, by itself, is not a workable solution since such anneals lead to the formation of pinholes (*vide infra*) that provide access points from which the structure is similarly hollowed. In stark contrast, Cu nanostructures protected by HfO_2 and TiO_2 coatings were able to withstand H_2O immersion, showing no ill effects for the 100 day duration studied (Figure 4d,e). Nanostructures with these two coatings

https://dx.doi.org/10.1021/acs.chemmater.0c02715
Chem. Mater. 2020, 32, 6788–6799

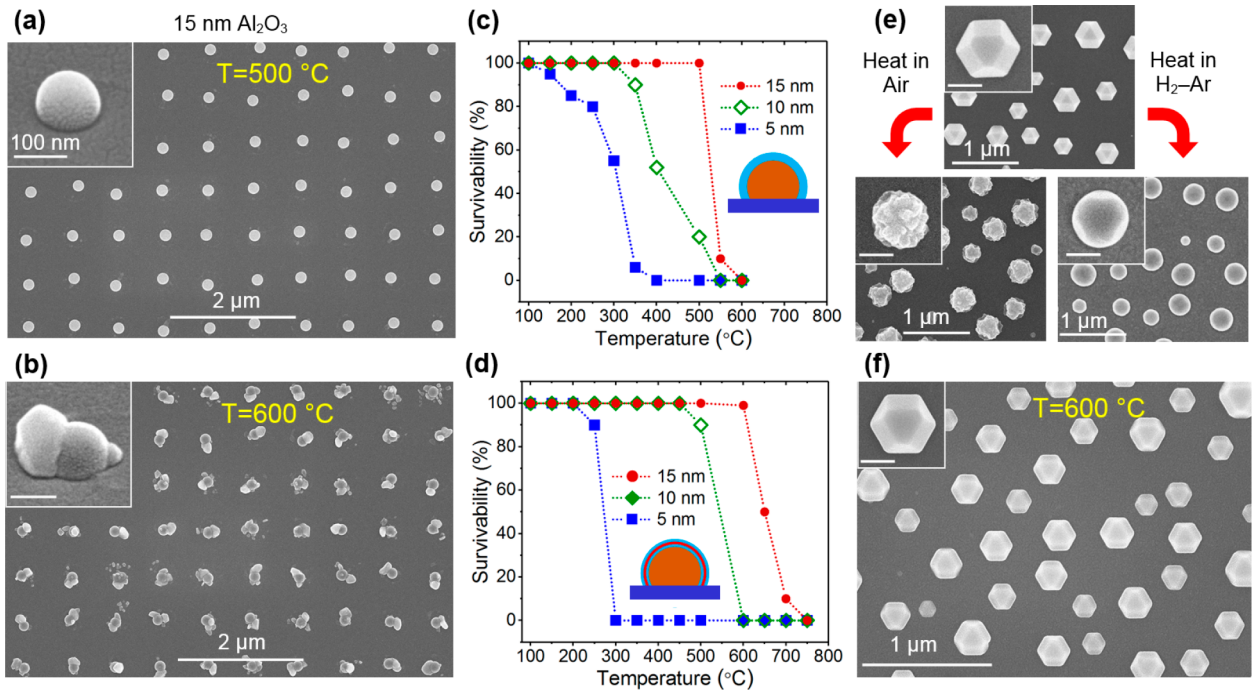

Figure 5. SEM images of Cu nanostructures coated with 15 nm of Al_2O_3 after being heated to (a) 500 °C and (b) 600 °C for 1 h where the latter has undergone catastrophic failure, while the former proved robust to the annealing temperature. Percent survivability vs annealing temperature for Cu nanostructures coated with various thicknesses of (c) Al_2O_3 and (d) Al_2O_3–HfO_2–Al_2O_3. (e) SEM images of highly faceted bare Cu nanostructure heated in air and in a H_2–Ar mixture. (f) Image of faceted structures with a 15 nm multilayer coating that withstood a 1 h heat treatment at 600 °C.

were also subjected to 1 M NaOH and HNO_3 to assess their chemical resistance to high and low pH environments (Figure S6). Only HfO_2 was able to withstand prolonged aggressive exposure to these extreme pH conditions, a result of potential significance to chemical sensing in highly corrosive environments.

Durability at Elevated Temperatures. Elevated temperatures represent a particularly challenging environment for metal nanostructures due to accelerated rates of oxidation and diffusion-induced morphological transformations. The LSPR for unprotected Cu nanostructures is, for example, completely extinguished in a mere 4 h when heated to 100 °C as the structures grow in size and develop irregular surface morphologies (Figure S7). Figure 5a–c summarizes the results obtained when Al_2O_3 coatings with thicknesses of 5, 10, and 15 nm were applied to arrayed Cu nanostructures and heated to various temperatures for 1 h. The 1 h time frame, while somewhat arbitrary, was chosen out of practicality to facilitate the testing of many samples. Figure 5a,b shows SEM images of a Al_2O_3-coated sample that proved robust when subjected to a 500 °C heat treatment and an identical sample that underwent catastrophic failure when heated to 600 °C. It is apparent from the morphology of the failed structures that the failure mode is one in which the Al_2O_3 shell is locally breached, creating a fissure through which material is extruded due to the volume expansion that occurs when Cu is suddenly exposed to high temperature oxidation processes. With the failure of individual structures being easily identified using SEM images, a statistical analysis of the nanostructure survivability as a function of both temperature and coating thickness was carried out. The results, shown in Figure 5c, reveal that coating thicknesses of 5, 10, and 15 nm can withstand temperatures of 100, 300, and 500 °C, respectively. These operational limits were confirmed through spectroscopic characterization that reveal that the LSPR of the Cu nanostructures remained intact as long as the integrity of the coating was maintained (Figure S8). This result rules out the possibility that significant Cu oxidation results from the diffusion of oxygen through the coating.

It is well-documented that ALD-deposited amorphous Al_2O_3, when heated, undergoes a densification that leads to surface roughening[74] and nanopore formation.[63,76] It is, therefore, likely that this same densification process is responsible for coating failure. Consistent with this conclusion is the fact that HfO_2 and TiO_2 coatings have significantly lower crystallization temperatures than Al_2O_3[66,77,78] and correspondingly fail at temperatures that are much lower. Studies of ALD-deposited films have also revealed that crystallization processes can be impeded in multilayer structures composed of Al_2O_3 and HfO_2.[79−81] These investigations, however, did not address whether the formation of such multilayers stabilizes the coating against pinhole formation. Studies were, therefore, undertaken that assessed Al_2O_3–HfO_2–Al_2O_3 coatings with total thicknesses of 5, 10, and 15 nm as a potential failure mitigation strategy where the three layers were of the same width (i.e., 1.67, 3.33, and 5 nm). The results, shown in Figure 5d, reveal that the multilayer structures can increase the thermal damage threshold over that of an Al_2O_3 coating by 100, 150, and 100 °C for coating thicknesses of 5, 10, and 15 nm, respectively. This finding not only demonstrates that triple-layer coatings offer Cu thermal protection at significantly higher temperatures but also points toward the large parameter space offered by multilayered structures (e.g., number of layers, layer thickness, oxide material) as a potential avenue for achieving enhanced performance.

In addition to oxidation, there is a strong tendency for metal nanostructures to morphologically reconfigure when

https://dx.doi.org/10.1021/acs.chemmater.0c02715
Chem. Mater. 2020, 32, 6788−6799

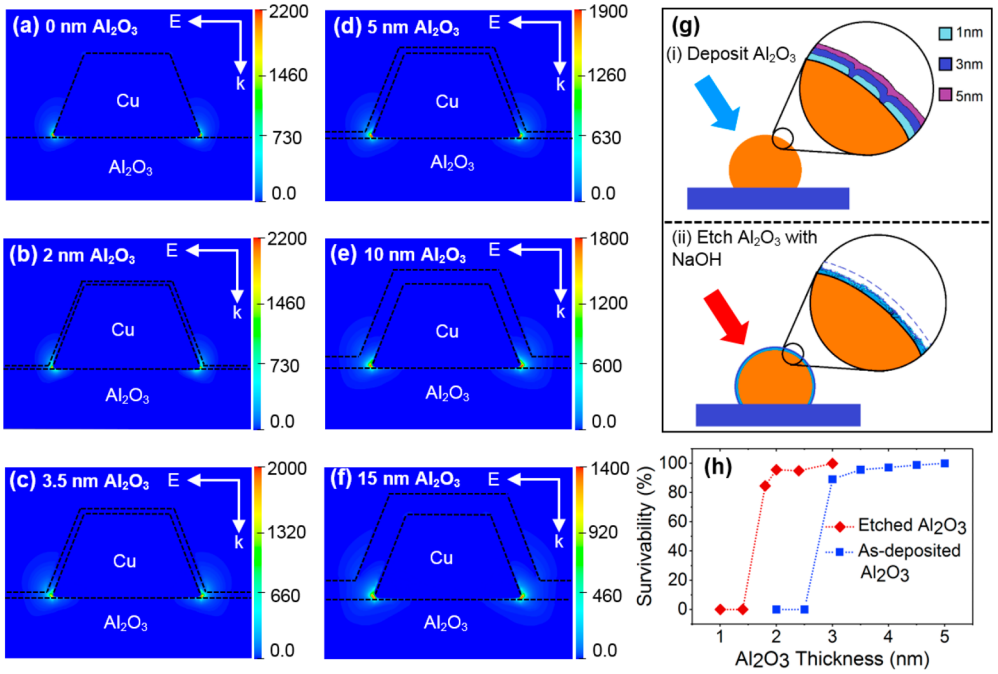

Figure 6. (a) Simulations of the near-field enhancements ($|\mathbf{E}/\mathbf{E}_0|^2$) for a 120 nm diameter substrate-truncated Cu cuboctahedron that is resting on a sapphire substrate. (b–f) Near-field enhancements for the same nanostructure when coated with Al_2O_3 shells of various thickness. (g) Schematic of the scheme used to obtain pinhole-free Al_2O_3 coatings with thicknesses that are less than that obtainable from as-deposited coatings. (h) Cu nanostructure survivability as a function of the coating thickness for as-deposited and etched Al_2O_3 layers.

heated.[24,25,27,28] With nanostructure properties being highly dependent on shape, this tendency is highly detrimental in that it can disrupt or destroy optical properties that were so carefully engineered in the first place and, in doing so, puts important applications at risk.[25−28] Figure 5e shows SEM images that demonstrate the morphological disruptions that occur when highly faceted bare Cu nanostructures are exposed to elevated temperatures in both air and a H_2–Ar gas mixture. Although both scenarios lead to morphological transformations, the latter is entirely due to surface diffusion processes that act to round the faceted structures. The deposition of an oxide coating onto faceted structures prior to heating will inevitably obstruct these surface diffusion pathways and, hence, act to preserve the nanostructure architecture when heated.[40,46] Thermal endurance testing carried out on faceted structures showed that both the Al_2O_3 and Al_2O_3–HfO_2–Al_2O_3 coatings maintained nanostructure faceting (Figure 5f) where the thermal damage threshold showed no obvious deviation from those presented in Figure 5c,d. The result indicates that the corners created by crisp faceting do not adversely influence the coating integrity.

Enhancing Plasmonic Near-Fields. The encapsulation of a plasmonic nanostructure within a pinhole-free oxide shell will inevitably disrupt the near-fields that develop near its surface when the LSPR is excited. The color maps shown in Figure 6a, obtained through DDA simulations, depict the near-fields of a one-third truncated Cu cuboctahedra for the cross section having the maximum near-field intensity when resonantly excited. Figure 6b–f shows the analogous maps for the same structures when coated with Al_2O_3 shells of various thickness. The bare structure shows maximum near-field intensities (i.e., hot spots) at the perimeter of the nanostructure where it meets the substrate, as is typical for a substrate-truncated structure.[82,83] This is due to the high curvature expressed by the nanostructure at the interfacial plane as well as the dielectric environment provided by the substrate. As the coating is applied and made progressively thicker, the near-fields undergo an evolution in which their overall spatial extent increases, but where the most intense near-fields become entrapped within shell boundaries. Similar trends are observed for substrate-truncated spheres, but where the near-fields are less intense (Figure S9). A positive aspect of these results is that sizable near-fields extend beyond the spatial extent of the coating for all cases. There is, nevertheless, an obvious downside to the application of coatings in terms of the plasmonic near-fields accessible, and as such, methods and processing conditions that are able to obtain thinner pinhole-free coatings are highly desirable.

The results presented in Figure 2d place a lower limit of 4.5 nm on the Al_2O_3 thickness needed to obtain pinhole-free shells in high yield for as-deposited ALD coatings. To circumvent this limit, a scheme was devised in which Al_2O_3 coatings were first deposited to a thickness of 5 nm so as to allow pinholes to fill in through lateral growth after which the shell was thinned using a NaOH etch (Figure 6g). To invoke such a strategy required that the Al_2O_3 etch rate be accurately determined. This was done through a series of experiments in which Al_2O_3 layers of various thicknesses were deposited on Cu nanostructures and then slowly etched away while spectroscopically monitoring the blue shift in the LSPR resulting from a thinning of the Al_2O_3 layer. The complete removal of the Al_2O_3 layer resulted in a spectroscopic signature characterized by a rapid decline in the rate of LSPR shift. The Al_2O_3 etch rate of 0.64 nm·min^{-1} was then extracted from a plot of the Al_2O_3 layer thickness vs etching time (Figure S10). With etching conditions identified, it is a straightforward procedure to prepare a series of identical Cu nanostructures with an initial Al_2O_3 coating thickness of 5 nm that are thinned to varying degrees and then perform acid etch tests to determine if shell integrity is preserved. Figure 6h shows a comparison of the

https://dx.doi.org/10.1021/acs.chemmater.0c02715
Chem. Mater. 2020, 32, 6788−6799

survivability data for Cu nanostructures with as-deposited shells with those obtained through the thinning procedure. The data clearly shows that the devised procedure allows for thinner shells. Although the thickness reduction obtained for Al_2O_3 coatings in absolute terms is only 2 nm, it should be understood that such changes can be of great significance since achievable SERS enhancement from a spherical nanoparticle of radius a decreases as $(1 + r/a)^{-10}$ where r is the distance between the absorbate and the plasmonic nanostructure.[84]

Broader Implications. From a broader perspective, it should be recognized that the strategies and processing science described herein are not specific to Cu nanostructures but could instead be applied to other vulnerable nanomaterials. Ag nanostructures, for example, tarnish in air,[85] are readily leached in aqueous environments,[86] are subject to shape changes when heated,[39] and could, thus, gain increased functionality if its surface were similarly protected. With Ag having far superior plasmonic properties, a sufficiently thin coating could lead to a trade-off whereby its somewhat diminished plasmonic response provides it with both durability and performance characteristics that exceed that of bare Au. Moreover, both Au and Ag could benefit from coatings that effectively stifle surface diffusion processes when heated and, as a result, nullify morphological disruptions including the dulling of the sharp corners that are crucial in obtaining high near-field intensities. Even if such solutions prove workable, Cu still has a price point advantage over its more noble metal counterparts. Additionally, its far greater sensitivity to environmental factors makes it a superior testbed for advancing coating solutions since aging effects are both accelerated and exaggerated. It should also be noted that the devised coating strategies share synergies with research directed toward the advancement of countermeasures that are able to combat the durability issues associated with colloidal nanostructures.[27,28,87,88]

Even though coatings offer solutions in terms of durability, their potential influence upon the performance of on-chip plasmonic devices cannot be overlooked. An examination of the most relevant plasmonic properties reveals both advantages and disadvantages. Both the thickness and dielectric properties of the coating material strongly influence the LSPR. Such influences must, therefore, be engineered into an overall solution so as to give rise to a plasmonic response that meets the demands of a particular application. It should, however, be noted that the fine control offered by ALD could prove advantageous in tuning the LSPR wavelength to a desired value even in a scenario where plasmonic nanostructure fabrication results in sample-to-sample variations. Plasmonic near-fields are inevitably diminished when a coating is applied, but where such influences could be partially mitigated by the coating's ability to preserve sharp corners and where the durability offered allows for the use of Ag as opposed to bare Au. The coating is also advantageous to near-field-based applications requiring a dielectric spacer (e.g., SHINERS, SHINEF).[29−32] Applications in which near-influences are to be felt within the substrate material (e.g., photovoltaics) will also be largely unaffected. Likewise, the hot electrons produced as the plasmon dephases can easily enter the substrate material. With a relatively low band gap, TiO_2 coatings could similarly allow for the injection of hot electrons into surrounding media,[20] a property that has been widely exploited as an enabler for plasmonic photochemistry.[89,90] Al_2O_3 and HfO_2 would, however, prove unsatisfactory as hot electron transport media. Photocatalytic reactions requiring an exposed metal surface are also unworkable. Plasmonic heating[91] could, in fact, benefit from the application of a coating because it results in an increased absorbance. Such benefits could, however, be offset by the thermal properties of the coating material. Moreover, the versatility of the ALD technique allows for the use of oxide materials beyond those described herein. Although SiO_2 is an obvious candidate,[92] its compatibility with Cu is questionable.[93] Taking all factors into account, the overall challenge is to effectively utilize coating materials in instances where application-specific trade-offs prove beneficial.

CONCLUSION

In summary, we have demonstrated that ultrathin oxide coatings, when applied to substrate-based Cu nanostructures, provide a level of durability that greatly exceeds that of unprotected structures. The work takes advantage of the fine controls and conformal coating capabilities offered by ALD. In doing so, a mainstream wafer-based processing technique is integrated with plasmonic nanostructure nanofabrication capabilities to achieve Cu-based photoactive surfaces with extraordinary resistance to environmental attack. Cu coating solutions have been advanced that are able to ensure long shell-lives, resist degradation while operating in air and H_2O, endure prolonged aggressive exposure to extreme pH environments, and resist oxidation and morphological transformations at temperatures as high as 600 °C. Although some plasmonic properties are inevitably diminished due to the presence of the coating, it can also be advantageous in that the coating can be used to fine-tune the plasmon resonance, preserve the sharp faceting that gives rise to hot spots, and act as a dielectric spacer in applications that demand one. Additionally, Al_2O_3 coatings are amenable to a thinning strategy that enhances the accessible near-fields, while TiO_2 coatings provide the means to transport hot electrons to the outside surface of the coating. With the potential for applying these and related strategies to other vulnerable nanomaterials such as Ag, there is the opportunity to bring otherwise inaccessible functionalities to the substrate surface and, in the process, broaden the scope of applications to which these nanomaterials can be applied.

EXPERIMENTAL SECTION

Chemicals and Materials. The Cu target used to sputter-deposit films was cut from a 0.5 mm thick foil with 99.9999% purity (Alfa Aesar). Two-side polished [0001]-oriented sapphire substrates were diced from a 100 mm diameter wafer (MTI Corp.). Cu nanostructures were assembled in an ultrahigh purity 10%−90% H_2−Ar gas mixture (Airgas). Nanoimprint lithography utilized stamps obtained from Lightsmyth Technologies, a trichloro(1H,1H,2H,2H-perfluorooctyl)silane antisticking layer (MilliporeSigma), and a 7030R thermal resist (Micro Resist Technology, GmbH). The ALD precursors trimethylaluminum (TMA) and tetrakis-(ethylmethylamido)hafnium (TEMAH) were sourced from MilliporeSigma, while tetrakis(dimethylamido)titanium (TDMAT) was obtained from SAFC Hitech. Solution-based synthesis utilized copper nitrate $(Cu(NO_3)_2$ (MilliporeSigma) and L-ascorbic acid (AA, MilliporeSigma). Durability tests were carried out using nitric acid (HNO_3, Alfa Aesar) and sodium hydroxide (NaOH, MilliporeSigma). Deionized (DI) water with a resistivity of 18.2 MΩ·cm was used for the preparation of all aqueous solutions. All chemicals were used as received.

Dewetted Cu Nanostructures with Random Size and Placement. Cu films with a thickness of 1.3 nm were sputter deposited at room temperature onto 5 mm × 10.5 mm × 0.6 mm [0001]-oriented sapphire substrates. Depositions proceeded at a rate of 9 nm·min^{-1} in 7 × 10^{-5} Torr of Ar using Penning ion gun current

https://dx.doi.org/10.1021/acs.chemmater.0c02715
Chem. Mater. 2020, 32, 6788−6799

and voltage settings of 200 μA and 6 keV. The coated substrate was removed from the sputter coater, placed in an alumina crucible, and inserted into a quartz tube furnace under a flowing 10%−90% H_2−Ar atmosphere. After a 30 min interval in which residual air was flushed from the quartz tube, the flow rate was reduced from 120 to 60 $cm^3 \cdot min^{-1}$, and the sample was heated to 900 °C in 22 min, held at this temperature for 3 min, and then rapidly cooled to room temperature in approximately 45 min. The Cu nanostructures produced, when removed from the furnace, were immediately subjected to the next processing step, characterization procedure, or durability test so as to minimize the influence of oxidation. In an effort to eliminate the possibility of cross contamination with other processes, all Cu dewetting procedures were carried out in a dedicated quartz tube and alumina crucible. The tube and crucible were baked before use.

Cu Cuboctahedra. Cu nanostructures with roundish morphologies were fabricated using the procedures outlined in the previous section, but where the Cu film thickness and maximum processing temperature were adjusted to values more conducive to the formation of equiaxed structures (i.e., 11 nm and 1040 °C).[57] Upon removal from the tube furnace, the Cu nanostructures were immediately subjected to a solution-based synthesis that, in a matter of minutes, transforms the near-spherical geometries into cuboctahedra. The synthesis begins by preparing 95 °C aqueous solutions of $Cu(NO_3)_2$ (3 mL, 1 mM) and AA (1 mL, 10 mM). The substrate-supported Cu nanostructures are inserted into the AA solution, and after a waiting period of 10 s, the $Cu(NO_3)_2$ is quickly added. The addition causes a chemical reaction to ensue that sees Cu^{2+} ions reduced by AA to form a neutral Cu^0 species that readily deposits onto the existing Cu nanostructures. After a 5 min interval, the substrate is removed, rinsed in DI H_2O, and dried under flowing N_2 gas. Details of the procedure can be found elsewhere.[57]

Periodic Arrays of Cu Nanostructures. Nanostructure arrays are formed using a benchtop nanofabrication procedure in which nanoimprint lithography is used to define periodic arrays of polycrystalline Cu discs that are then exposed to a heating regimen that causes each disc to assemble into a single-crystal nanostructure. The lithographic steps, which are described in detail elsewhere,[60,94] proceed by spin coating a 400 nm thick moldable polymeric resist onto a 10 mm × 10.5 mm × 0.6 mm sapphire substrate, embossing it with a commercially available silicon stamp expressing a square pattern of nanocylinders (length = 350 nm, diameter = 260 nm, pitch = 700 nm), and then exposing the imprinted resist to a reactive ion etching (RIE) treatment that creates openings to the substrate surface at the embossed sites. A 15 nm thick layer of Cu is then sputter-deposited over the entire surface. This is followed by a lift-off procedure that dissolves the resist and removes the Cu that once resided on the surface of the resist, leaving behind an array of Cu discs on the substrate surface. The arrayed structures are inserted into a tube furnace and exposed to the same heating regimen as described in the previous section. Upon removal from the tube furnace, arrays were often cleaved into smaller pieces to facilitate their immediate use in multiple experiments.

Atomic Layer Deposition. A Cambridge NanoTech Savannah 100 ALD system was used to deposit the Al_2O_3 and HfO_2 coatings, while an Oxford FlexAl system was used for TiO_2. The key differences between the two systems are that the Oxford instrument has a lower base pressure (1 vs 270 mTorr) and is equipped with a load lock to facilitate sample insertion and removal. In an effort to mitigate any Cu oxidation stemming from the higher base pressure in the Savannah, the depositions were expedited by initially purging the system with N_2 gas for 60 s at 5 times the flow rate used during the deposition (i.e., 100 sccm). The flow is then reduced to 20 sccm over the course of 10 s followed by the immediate initiation of the deposition through the introduction of the first precursor. TMA, TEMAH, and TDMAT were used as the Al, Hf, and Ti precursors, respectively, while H_2O was used as the oxidant for all three cases. Growth cycles for Al_2O_3 utilized alternating 20 ms exposures of Al_2O_3 and H_2O separated by a 7 s N_2 gas purge. HfO_2 depositions proceeded in much the same manner except that a longer pulse time of 150 ms was used for TEMAH, and the N_2 purge time was increased to 10 s. TiO_2 utilized TDMAT and H_2O pulse times of 800 ms and 1 s, respectively, separated by a purge time of 7 s and a 3 s pumping interval. The deposition temperature for all three oxides is 200 °C. These processing parameters resulted in deposition rates of 1.0, 0.9, and 0.25 Å/cycle for Al_2O_3, HfO_2, and TiO_2, respectively. The Al_2O_3−HfO_2−Al_2O_3 triple layer coatings, used to obtain the data in Figure 5d, were deposited using the same conditions, but where an extended purge time of 60 s was used when switching from one oxide growth to another. Table S1 of the Supporting Information summarizes all the relevant parameters associated with the ALD depositions. The etch tests used to determine whether ALD-deposited coatings are pinhole-free (Figure 2d−f) proceeded by exposing the structures to 1 M HNO_3 for 20 min.

Simulations. DDA simulations[70] utilized the DDSCAT 7.3 software package. The simulated geometries were designed and visualized using LAMMPS and Visual Molecular Dynamics (VMD) software packages, respectively. For all simulations, the total number of dipoles defining the nanostructure−coating−substrate system was approximately 270000. The dielectric constants for ALD-deposited Al_2O_3 were taken from the work of Groner et al.,[62] while those associated with Cu and the sapphire substrate utilized well-accepted sources. The simulated Cu structures used to obtain the data in Figure 6a−f had a point-to-point diameter of 120 nm and a truncation factor[82] of one-third. The color maps show the $|\mathbf{E}/\mathbf{E}_0|^2$ values occurring at the resonant wavelength for nanostructure cross sections taken through the structure in the direction of light polarization.

Instrumentation. Cu was sputter deposited in a Model 681 Gatan high resolution ion beam coater. Nanoimprint lithography utilized a (i) Laurell Spin Coater, (ii) SAMCO RIE-1C Reactive Ion Etcher, and (ii) home-built press.[60] ALD depositions were performed using a Cambridge Savannah S100 or an Oxford FlexAl System. Coating thicknesses were measured with a Gaertner L116S ellipsometer. LSPR spectra were recorded using a JASCO V-730 UV−visible spectrophotometer. SEM images were obtained using a Magellan 400 FEI field emission scanning electron microscope (FESEM). XRD spectra were recorded using a Bruker D8 Advance diffractometer.

■ ASSOCIATED CONTENT

Supporting Information

The Supporting Information is available free of charge at https://pubs.acs.org/doi/10.1021/acs.chemmater.0c02715.

Additional characterization, simulations, and ALD deposition conditions (PDF)

■ AUTHOR INFORMATION

Corresponding Author

Svetlana Neretina − *College of Engineering and Department of Chemistry & Biochemistry, University of Notre Dame, Notre Dame, Indiana 46556, United States;* orcid.org/0000-0002-6889-4384; Email: sneretina@nd.edu

Authors

Arin S. Preston − *College of Engineering, University of Notre Dame, Notre Dame, Indiana 46556, United States*

Robert A. Hughes − *College of Engineering, University of Notre Dame, Notre Dame, Indiana 46556, United States*

Trevor B. Demille − *College of Engineering, University of Notre Dame, Notre Dame, Indiana 46556, United States*

Complete contact information is available at: https://pubs.acs.org/10.1021/acs.chemmater.0c02715

Notes

The authors declare no competing financial interest.

https://dx.doi.org/10.1021/acs.chemmater.0c02715
Chem. Mater. 2020, 32, 6788−6799

■ ACKNOWLEDGMENTS

This work is supported by a National Science Foundation Award (CMMI-1911991) to S.N. It has also benefited from the facilities available through the Notre Dame Nanofabrication Facility (NDNF), the Notre Dame Integrated Imaging Facility (NDIIF), and the Notre Dame Molecular Structure Facility (NDMSF). The authors are grateful to and acknowledge the expertise of M. Richmond in the preparation of oxide coatings using ALD. The authors are also grateful to S. Shinde (ND Energy, Notre Dame) for the early stage discussions that motivated this work.

■ REFERENCES

(1) Gu, Z.; Shen, H.; Shang, L.; Lv, X.; Qian, L.; Zheng, G. Nanostructured Copper-Based Electrocatalysts for CO_2 Reduction. *Small Methods* **2018**, *2*, 1800121.

(2) Christoforidis, K. C.; Fornasiero, P. Photocatalysis for Hydrogen Production and CO_2 Reduction: The Case of Copper-Catalysts. *ChemCatChem* **2019**, *11*, 368−382.

(3) Feng, Y.; Zhu, J. Copper Nanomaterials and Assemblies for Soft Electronics. *Sci. China Mater.* **2019**, *62*, 1679−1708.

(4) Hsu, P.-C.; Wu, H.; Carney, T. J.; McDowell, M. T.; Yang, Y.; Garnett, E. C.; Li, M.; Hu, L.; Cui, Y. Passivation Coating on Electrospun Copper Nanofibers for Stable Transparent Electrodes. *ACS Nano* **2012**, *6*, 5150−5156.

(5) Ye, S.; Rathmell, A. R.; Chen, Z.; Stewart, I. E.; Wiley, B. J. Metal Nanowire Networks: The Next Generation of Transparent Conductors. *Adv. Mater.* **2014**, *26*, 6670−6687.

(6) Cui, F.; Yu, Y.; Dou, L.; Sun, J.; Yang, Q.; Schildknecht, C.; Schierle-Arndt, K.; Yang, P. Synthesis of Ultrathin Copper Nanowires Using Tris(trimethylsilyl)silane for High-Performance and Low-Haze Transparent Conductors. *Nano Lett.* **2015**, *15*, 7610−7615.

(7) Markin, A. V.; Markina, N. E.; Popp, J.; Cialla-May, D. Copper Nanostructures for Chemical Analysis using Surface-Enhanced Raman Spectroscopy. *TrAC, Trends Anal. Chem.* **2018**, *108*, 247−259.

(8) Sugawa, K.; Tamura, T.; Tahara, H.; Yamaguchi, D.; Akiyama, T.; Otsuki, J.; Kusaka, Y.; Fukuda, N.; Ushijima, H. Metal-Enhanced Fluorescence Platforms Based on Plasmonic Ordered Copper Arrays: Wavelength Dependence of Quenching and Enhancement Effects. *ACS Nano* **2013**, *7*, 9997−10010.

(9) Pereira, A. J.; Gomes, J. P.; Lenz, G. F.; Schneider, R.; Chaker, J. A.; de Souza, P. E. N.; Felix, J. F. Facile Shape-Controlled Fabrication of Copper Nanostructures on Borophosphate Glasses: Synthesis, Characterization, and Their Highly Sensitive Surface-Enhanced Raman Scattering (SERS) Properties. *J. Phys. Chem. C* **2016**, *120*, 12265−12272.

(10) Gawande, M. B.; Goswami, A.; Felpin, F.-X.; Asefa, T.; Huang, X.; Silva, R.; Zou, X.; Zboril, R.; Varma, R. S. Cu and Cu-Based Nanoparticles: Synthesis and Applications in Catalysis. *Chem. Rev.* **2016**, *116*, 3722−3811.

(11) Zheng, P.; Tang, H.; Liu, B.; Kasani, S.; Huang, L.; Wu, N. Origin of Strong and Narrow Localized Surface Plasmon Resonance of Copper Nanocubes. *Nano Res.* **2019**, *12*, 63−68.

(12) Iyengar, P.; Huang, J.; De Gregorio, G. L.; Gadiyar, C.; Buonsanti, R. Size Dependent Selectivity of Cu Nano-Octahedra Catalysts for the Electrochemical Reduction of CO_2 to CH_4. *Chem. Commun.* **2019**, *55*, 8796−8799.

(13) Lyu, Z.; Xie, M.; Gilroy, K. D.; Hood, Z. D.; Zhao, M.; Zhou, S.; Liu, J.; Xia, Y. A Rationally Designed Route to the One-Pot Synthesis of Right Bipyramidal Nanocrystals of Copper. *Chem. Mater.* **2018**, *30*, 6469−6477.

(14) Lee, J.-W.; Han, J.; Lee, D. S.; Bae, S.; Lee, S. H.; Lee, S.-K.; Moon, B. J.; Choi, C.-J.; Wang, G.; Kim, T.-W. 2D Single-Crystalline Copper Nanoplates As a Conductive Filler for Electronic Ink Applications. *Small* **2018**, *14*, 1703312.

(15) Luo, M.; Ruditskiy, A.; Peng, H.-C.; Tao, J.; Figueroa-Cosme, L.; He, Z.; Xia, Y. Penta-Twinned Copper Nanorods: Facile Synthesis *via* Seed-Mediated Growth and Their Tunable Plasmonic Properties. *Adv. Funct. Mater.* **2016**, *26*, 1209−1216.

(16) Lu, S.-C.; Hsiao, M.-C.; Yorulmaz, M.; Wang, L.-Y.; Yang, P.-Y.; Link, S.; Chang, W.-S.; Tuan, H.-Y. Single-Crystalline Copper Nano-Octahedra. *Chem. Mater.* **2015**, *27*, 8185−8188.

(17) Pastoriza-Santos, I.; Sánchez-Iglesias, A.; Rodríguez-González, B.; Liz-Marzán, L. M. Aerobic Synthesis of Cu Nanoplates with Intense Plasmon Resonances. *Small* **2009**, *5*, 440−443.

(18) Chan, G. H.; Zhao, J.; Hicks, E. M.; Schatz, G. C.; Van Duyne, R. P. Plasmonic Properties of Copper Nanoparticles Fabricated by Nanosphere Lithography. *Nano Lett.* **2007**, *7*, 1947−1952.

(19) Cai, Y.-Y.; Collins, S. S. E.; Gallagher, M. J.; Bhattacharjee, U.; Zhang, R.; Chow, T. H.; Ahmadivand, A.; Ostovar, B.; Al-Zubeidi, A.; Wang, J.; Nordlander, P.; Landes, C. F.; Link, S. Single-Particle Emission Spectroscopy Resolves d-Hole Relaxation in Copper Nanocubes. *ACS Energy Lett.* **2019**, *4*, 2458−2465.

(20) Lee, C.; Park, Y.; Park, J. Y. Hot Electrons Generated by Intraband and Interband Transition Detected using a Plasmonic Cu/TiO_2 Nanodiode. *RSC Adv.* **2019**, *9*, 18371−18376.

(21) Naik, G. V.; Shalaev, V. M.; Boltasseva, A. Alternative Plasmonic Materials: Beyond Gold and Silver. *Adv. Mater.* **2013**, *25*, 3264−3294.

(22) West, P. R.; Ishii, S.; Naik, G. V.; Emani, N. K.; Shalaev, V. M.; Boltasseva, A. Searching for Better Plasmonic Materials. *Laser Photonics Rev.* **2010**, *4*, 795−808.

(23) Kautzky, M. C.; Blaber, M. G. Materials for Heat-Assisted Magnetic Recording Heads. *MRS Bull.* **2018**, *43*, 100−105.

(24) Huang, W.; Qian, W.; El-Sayed, M. A. Gold Nanoparticles Propulsion from Surface Fueled by Absorption of Femtosecond Laser Pulse at Their Surface Plasmon Resonance. *J. Am. Chem. Soc.* **2006**, *128*, 13330−13331.

(25) Li, W.; Guler, U.; Kinsey, N.; Naik, G. V.; Boltasseva, A.; Guan, J.; Shalaev, V. M.; Kildishev, A. V. Refractory Plasmonics with Titanium Nitride: Broadband Metamaterial Absorber. *Adv. Mater.* **2014**, *26*, 7959−7965.

(26) Guler, U.; Boltasseva, A.; Shalaev, V. M. Refractory Plasmonics. *Science* **2014**, *344*, 263−264.

(27) Wang, L.; Wang, L.; Meng, X.; Xiao, F.-S. New Strategies for the Preparation of Sinter-Resistant Metal-Nanoparticle-Based Catalysts. *Adv. Mater.* **2019**, *31*, 1901905.

(28) Dai, Y.; Lu, P.; Cao, Z.; Campbell, C. T.; Xia, Y. The Physical Chemistry and Materials Science behind Sinter-Resistant Catalysts. *Chem. Soc. Rev.* **2018**, *47*, 4314−4331.

(29) Ding, S.-Y.; Yi, J.; Li, J.-F.; Ren, B.; Wu, D.-Y.; Panneerselvam, R.; Tian, Z.-Q. Nanostructure-Based Plasmon-Enhanced Raman Spectroscopy for Surface Analysis of Materials. *Nat. Rev. Mater.* **2016**, *1*, 16021.

(30) Li, J. F.; Huang, Y. F.; Ding, Y.; Yang, Z. L.; Li, S. B.; Zhou, X. S.; Fan, F. R.; Zhang, W.; Zhou, Z. Y.; Wu, D. Y.; Ren, B.; Wang, Z. L.; Tian, Z. Q. Shell-Isolated Nanoparticle-Enhanced Raman Spectroscopy. *Nature* **2010**, *464*, 392−395.

(31) Krajczewski, J.; Kudelski, A. Shell-Isolated Nanoparticle-Enhanced Raman Spectroscopy. *Front. Chem.* **2019**, *7*, 410.

(32) Langer, J.; de Aberasturi, D. J.; Aizpurua, J.; Alvarez-Puebla, R. A.; Auguie′, B.; Baumberg, J. J.; Bazan, G. C.; Bell, S. E. J.; Boisen, A.; Brolo, A. G.; Choo, J.; Cialla-May, D.; Deckert, V.; Fabris, L.; Faulds, K.; García de Abajo, F. J.; Goodacre, R.; Graham, D.; Haes, A. J.; Haynes, C. L.; et al. Present and Future of Surface-Enhanced Raman Scattering. *ACS Nano* **2020**, *14*, 28−117.

(33) Li, J.-F.; Li, C.-Y.; Aroca, R. F. Plasmon-Enhanced Fluorescence Spectroscopy. *Chem. Soc. Rev.* **2017**, *46*, 3962−3979.

(34) Dong, J.; Zhang, Z.; Zheng, H.; Sun, M. Recent Progress on Plasmon-Enhanced Fluorescence. *Nanophotonics* **2015**, *4*, 472−490.

(35) Fang, P.-P.; Lu, X.; Liu, H.; Tong, Y. Applications of Shell-Isolated Nanoparticles in Surface-Enhanced Raman Spectroscopy and Fluorescence. *TrAC, Trends Anal. Chem.* **2015**, *66*, 103−117.

(36) Gérard, D.; Gray, S. K. Aluminium Plasmonics. *J. Phys. D: Appl. Phys.* **2015**, *48*, 184001.

https://dx.doi.org/10.1021/acs.chemmater.0c02715
Chem. Mater. 2020, 32, 6788−6799

(37) Knight, M. W.; King, N. S.; Liu, L.; Everitt, H. O.; Nordlander, P.; Halas, N. J. Aluminum for Plasmonics. *ACS Nano* **2014**, *8*, 834−840.
(38) Prakash, J.; Swart, H. C.; Zhang, G.; Sun, S. Emerging Applications of Atomic Layer Deposition for the Rational Design of Novel Nanostructures for Surface-Enhanced Raman Scattering. *J. Mater. Chem. C* **2019**, *7*, 1447−1471.
(39) Albrecht, G.; Ubl, M.; Kaiser, S.; Giessen, H.; Hentschel, M. Comprehensive Study of Plasmonic Materials in the Visible and Near-Infrared: Linear, Refractory, and Nonlinear Optical Properties. *ACS Photonics* **2018**, *5*, 1058−1067.
(40) Ma, L.; Huang, Y.; Hou, M.; Xie, Z.; Zhang, Z. Silver Nanorods Wrapped with Ultrathin Al_2O_3 Layers Exhibiting Excellent SERS Sensitivity and Outstanding SERS Stability. *Sci. Rep.* **2015**, *5*, 12890.
(41) Im, H.; Oh, S.-H. Oxidation Sharpening, Template Stripping, and Passivation of Ultra-Sharp Metallic Pyramids and Wedges. *Small* **2014**, *10*, 680−684.
(42) Wang, X.; Santschi, C.; Martin, O. J. F. Strong Improvement of Long-Term Chemical and Thermal Stability of Plasmonic Silver Nanoantennas and Films. *Small* **2017**, *13*, 1700044.
(43) Mazzotta, F.; Johnson, T. W.; Dahlin, A. B.; Shaver, J.; Oh, S.-H.; Höök, F. Influence of the Evanescent Field Decay Length on the Sensitivity of Plasmonic Nanodisks and Nanoholes. *ACS Photonics* **2015**, *2*, 256−262.
(44) Im, H.; Lindquist, N. C.; Lesuffleur, A.; Oh, S.-H. Atomic Layer Deposition of Dielectric Overlayers for Enhancing the Optical Properties and Chemical Stability of Plasmonic Nanoholes. *ACS Nano* **2010**, *4*, 947−954.
(45) Nugroho, F. A. A.; Albinsson, D.; Antosiewicz, T. J.; Langhammer, C. Plasmonic Metasurface for Spatially Resolved Optical Sensing in Three Dimensions. *ACS Nano* **2020**, *14*, 2345−2353.
(46) Albrecht, G.; Kaiser, S.; Giessen, H.; Hentschel, M. Refractory Plasmonics without Refractory Materials. *Nano Lett.* **2017**, *17*, 6402−6408.
(47) Li, Y.-F.; Dong, F.-X.; Chen, Y.; Zhang, X.-L.; Wang, L.; Bi, Y.-G.; Tian, Z.-N.; Liu, Y.-F.; Feng, J.; Sun, H.-B. As-Grown Graphene/Copper Nanoparticles Hybrid Nanostructures for Enhanced Intensity and Stability of Surface Plasmon Resonance. *Sci. Rep.* **2016**, *6*, 37190.
(48) Duan, J.; Liu, J.; Zhang, Y.; Trautmann, C.; Lei, D. Y. Surface Plasmonic Spectroscopy Revealing the Oxidation Dynamics of Copper Nanowires Embedded in Polycarbonate Ion-Track Templates. *J. Mater. Chem. C* **2016**, *4*, 3956−3962.
(49) Johnson, R. W.; Hultqvist, A.; Bent, S. F. A Brief Review of Atomic Layer Deposition: From Fundamentals to Applications. *Mater. Today* **2014**, *17*, 236−246.
(50) Wang, D.-D.; Ge, C.-W.; Wu, G.-A.; Li, Z.-P.; Wang, J.-Z.; Zhang, T.-F.; Yu, Y.-Q.; Luo, L.-B. A Sensitive Red Light Nano-Photodetector Propelled by Plasmonic Copper Nanoparticles. *J. Mater. Chem. C* **2017**, *5*, 1328−1335.
(51) Yang, H. J.; He, S.-Y.; Chen, H.-L.; Tuan, H.-Y. Monodisperse Copper Nanocubes: Synthesis, Self-Assembly, and Large-Area Dense-Packed Films. *Chem. Mater.* **2014**, *26*, 1785−1793.
(52) Preston, A. S.; Hughes, R. A.; Demille, T. B.; Neretina, S. Copper Template Design for the Synthesis of Bimetallic Copper−Rhodium Nanoshells through Galvanic Replacement. *Part. Part. Syst. Charact.* **2018**, *35*, 1700420.
(53) Kim, J.; Ju, T.-S.; Song, S.; Lee, D.; Cho, S. Y.; Bu, S. D.; Ko, W.; Li, A.-P.; Park, J.; Park, S. Enhancing the Local Conductivity of Cu Films Using Temperature-Assisted Agglomerated Cu Nanostructures. *J. Phys. D: Appl. Phys.* **2020**, *53*, 09LT02.
(54) Wu, Y.; Fowlkes, J. D.; Rack, P. D.; Diez, J. A.; Kondic, L. On the Breakup of Patterned Nanoscale Copper Rings into Droplets *via* Pulsed-Laser-Induced Dewetting: Competing Liquid-Phase Instability and Transport Mechanisms. *Langmuir* **2010**, *26*, 11972−11979.
(55) Curiotto, S.; Chien, H.; Meltzman, H.; Wynblatt, P.; Rohrer, G. S.; Kaplan, W. D.; Chatain, D. Orientation Relationships of Copper Crystals on c-Plane Sapphire. *Acta Mater.* **2011**, *59*, 5320−5331.
(56) Thompson, C. V. Solid-State Dewetting of Thin Films. *Annu. Rev. Mater. Res.* **2012**, *42*, 399−434.
(57) Preston, A. S.; Hughes, R. A.; Demille, T. B.; Rey Davila, V. M.; Neretina, S. Dewetted Nanostructures of Gold, Silver, Copper, and Palladium with Enhanced Faceting. *Acta Mater.* **2019**, *165*, 15−25.
(58) Neretina, S.; Hughes, R. A.; Gilroy, K. D.; Hajfathalian, M. Noble Metal Nanostructure Synthesis at the Liquid−Substrate Interface: New Structures, New Insights, and New Possibilities. *Acc. Chem. Res.* **2016**, *49*, 2243−2250.
(59) Hughes, R. A.; Menumerov, E.; Neretina, S. When Lithography Meets Self-Assembly: A Review of Recent Advances in the Directed Assembly of Complex Metal Nanostructures on Planar and Textured Surfaces. *Nanotechnology* **2017**, *28*, 282002.
(60) Menumerov, E.; Golze, S. D.; Hughes, R. A.; Neretina, S. Arrays of Highly Complex Noble Metal Nanostructures using Nanoimprint Lithography in Combination with Liquid-Phase Epitaxy. *Nanoscale* **2018**, *10*, 18186−18194.
(61) George, S. M. Atomic Layer Deposition: An Overview. *Chem. Rev.* **2010**, *110*, 111−131.
(62) Groner, M. D.; Fabreguette, F. H.; Elam, J. W.; George, S. M. Low-Temperature Al_2O_3 Atomic Layer Deposition. *Chem. Mater.* **2004**, *16*, 639−645.
(63) Karwal, S.; Li, T.; Yanguas-Gil, A.; Canlas, C. P.; Lei, Y.; Mane, A. U.; Libera, J. A.; Seifert, S.; Winans, R. E.; Elama, J. W. Tailoring Nanopore Formation in Atomic Layer Deposited Ultrathin Films. *J. Vac. Sci. Technol., A* **2018**, *36*, 01A103.
(64) Kukli, K.; Ritala, M.; Sajavaara, T.; Keinonen, J.; Leskelä, M. Atomic Layer Deposition of Hafnium Dioxide Films from Hafnium Tetrakis(ethylmethylamide) and Water. *Chem. Vap. Deposition* **2002**, *8*, 199−204.
(65) Liu, X.; Ramanathan, S.; Longdergan, A.; Srivastava, A.; Lee, E.; Seidel, T. E.; Barton, J. T.; Pang, D.; Gordon, R. G. ALD of Hafnium Oxide Thin Films from Tetrakis(ethylmethylamino)hafnium and Ozone. *J. Electrochem. Soc.* **2005**, *152*, G213−G219.
(66) Niemelä, J.-P.; Marin, G.; Karppinen, M. Titanium Dioxide Thin Films by Atomic Layer Deposition: A Review. *Semicond. Sci. Technol.* **2017**, *32*, 093005.
(67) Reiners, M.; Xu, K.; Aslam, N.; Devi, A.; Waser, R.; Hoffmann-Eifert, S. Growth and Crystallization of TiO_2 Thin Films by Atomic Layer Deposition Using a Novel Amido Guanidinate Titanium Source and Tetrakis-Dimethylamido-Titanium. *Chem. Mater.* **2013**, *25*, 2934−2943.
(68) Martínez, F. L.; Toledano-Luque, M.; Gandía, J. J.; Cárabe, J.; Bohne, W.; Röhrich, J.; Strub, E.; Mártil, I. Optical Properties and Structure of HfO_2 Thin Films Grown by High Pressure Reactive Sputtering. *J. Phys. D: Appl. Phys.* **2007**, *40*, 5256−5265.
(69) Kang, M.; Kim, S. W.; Park, H. Y. Optical Properties of TiO_2 Thin films with Crystal Structure. *J. Phys. Chem. Solids* **2018**, *123*, 266−270.
(70) Draine, B. T.; Flatau, P. J. Discrete-Dipole Approximation for Scattering Calculations. *J. Opt. Soc. Am. A* **1994**, *11*, 1491−1499.
(71) Dung Dang, T. M.; Le, T. T. T.; Fribourg-Blanc, E.; Dang, M. C. The Influence of Solvents and Surfactants on the Preparation of Copper Nanoparticles by a Chemical Reduction Method. *Adv. Nat. Sci.: Nanosci. Nanotechnol.* **2011**, *2*, 025004.
(72) Tsuji, M.; Yamaguchi, D.; Matsunaga, M.; Alam, J. Epitaxial Growth of Au@Cu Core-Shell Nanocrystals Prepared Using the PVP-Assisted Polyol Reduction Method. *Cryst. Growth Des.* **2010**, *10*, 5129−5135.
(73) Pacioni, N. L.; Filippenko, V.; Presseau, N.; Scaiano, J. C. Oxidation of Copper Nanoparticles in Water: Mechanistic Insights Revealed by Oxygen Uptake and Spectroscopic Methods. *Dalton Trans.* **2013**, *42*, 5832−5838.
(74) Broas, M.; Kanninen, O.; Vuorinen, V.; Tilli, M.; Paulasto-Kröckel, M. Chemically Stable Atomic-Layer-Deposited Al_2O_3 Films for Processability. *ACS Omega* **2017**, *2*, 3390−3398.
(75) Correa, G. C.; Bao, B.; Strandwitz, N. C. Chemical Stability of Titania and Alumina Thin Films Formed by Atomic Layer Deposition. *ACS Appl. Mater. Interfaces* **2015**, *7*, 14816−14821.

https://dx.doi.org/10.1021/acs.chemmater.0c02715
Chem. Mater. 2020, 32, 6788−6799

(76) Li, T.; Karwal, S.; Aoun, B.; Zhao, H.; Ren, Y.; Canlas, C. P.; Elam, J. W.; Winans, R. E. Exploring Pore Formation of Atomic Layer-Deposited Overlayers by *in Situ* Small- and Wide-Angle X ray Scattering. *Chem. Mater.* **2016**, *28*, 7082−7087.
(77) Zhang, L.; Jiang, H. C.; Liu, C.; Dong, J. W.; Chow, P. Annealing of Al_2O_3 Thin Films Prepared by Atomic Layer Deposition. *J. Phys. D: Appl. Phys.* **2007**, *40*, 3707−3713.
(78) Belo, G. S.; Nakagomi, F.; Minko, A.; da Silva, S. W.; Morais, P. C.; Buchanan, D. A. Phase Transition in Sputtered HfO_2 Thin Films: A Qualitative Raman Study. *Appl. Surf. Sci.* **2012**, *261*, 727−729.
(79) Nie, X.; Ma, D.; Ma, F.; Xu, K. Thermal Stability, Structural and Electrical Characteristics of the Modulated HfO_2/Al_2O_3 Films Fabricated by Atomic Layer Deposition. *J. Mater. Sci.* **2017**, *52*, 11524−11536.
(80) Lisiansky, M.; Popov, I.; Uvarov, V.; Korchnoy, V.; Meyler, B.; Yofis, S.; Shneider, Y. High-Voltage Metal-Insulator-Metal Capacitor Based on Crystalline $HfAlO_x$ Film Grown by Atomic Layer Deposition. *J. Vac. Sci. Technol., B: Nanotechnol. Microelectron.: Mater., Process., Meas., Phenom.* **2019**, *37*, 011209.
(81) Kukli, K.; Kemell, M.; Castán, H.; Dueñas, S.; Seemen, H.; Rähn, M.; Link, J.; Stern, R.; Ritala, M.; Leskelä, M. Atomic Layer Deposition and Properties of HfO_2-Al_2O_3 Nanolaminates. *ECS J. Solid State Sci. Technol.* **2018**, *7*, P501−P508.
(82) Demille, T. B.; Hughes, R. A.; Neretina, S. Periodic Arrays of Dewetted Silver Nanostructures on Sapphire and Quartz: Effect of Substrate Truncation on the Localized Surface Plasmon Resonance and Near-Field Enhancement. *J. Phys. Chem. C* **2019**, *123*, 19879−19886.
(83) Li, G.; Cherqui, C.; Wu, Y.; Bigelow, N. W.; Simmons, P. D.; Rack, P. D.; Masiello, D. J.; Camden, J. P. Examining Substrate-Induced Plasmon Mode Splitting and Localization in Truncated Silver Nanospheres with Electron Energy Loss Spectroscopy. *J. Phys. Chem. Lett.* **2015**, *6*, 2569−2576.
(84) Pilot, R.; Signorini, R.; Durante, C.; Orian, L.; Bhamidipati, M.; Fabris, L. A Review on Surface-Enhanced Raman Scattering. *Biosensors* **2019**, *9*, 57.
(85) Wang, X.; Santschi, C.; Martin, O. J. F. Strong Improvement of Long-Term Chemical and Thermal Stability of Plasmonic Silver Nanoantennas and Films. *Small* **2017**, *13*, 1700044.
(86) Menumerov, E.; Hughes, R. A.; Golze, S. D.; Neal, R. D.; Demille, T. B.; Campanaro, J. C.; Kotesky, K. C.; Rouvimov, S.; Neretina, S. Identifying the True Catalyst in the Reduction of 4-Nitrophenol: A Case Study Showing the Effect of Leaching and Oxidative Etching using Ag Catalysts. *ACS Catal.* **2018**, *8*, 8879−8888.
(87) Kang, H.; Buchman, J. T.; Rodriguez, R. S.; Ring, H. L.; He, J.; Bantz, K. C.; Haynes, C. L. Stabilization of Silver and Gold Nanoparticles: Preservation and Improvement of Plasmonic Functionalities. *Chem. Rev.* **2019**, *119*, 664−699.
(88) Crane, C. C.; Wang, F.; Li, J.; Tao, J.; Zhu, Y.; Chen, J. Synthesis of Copper−Silica Core−Shell Nanostructures with Sharp and Stable Localized Surface Plasmon Resonance. *J. Phys. Chem. C* **2017**, *121*, 5684−5692.
(89) Zhang, Y.; He, S.; Guo, W.; Hu, Y.; Huang, J.; Mulcahy, J. R.; Wei, W. D. Surface-Plasmon-Driven Hot Electron Photochemistry. *Chem. Rev.* **2018**, *118*, 2927−2954.
(90) Zhan, C.; Chen, X.-J.; Yi, J.; Li, J.-F.; Wu, D.-Y.; Tian, Z.-Q. From Plasmon-Enhanced Molecular Spectroscopy to Plasmon-Mediated Chemical Reactions. *Nat. Rev. Chem.* **2018**, *2*, 216−230.
(91) Jauffred, L.; Samadi, A.; Klingberg, H.; Bendix, P. M.; Oddershede, L. B. Plasmonic Heating of Nanostructures. *Chem. Rev.* **2019**, *119*, 8087−8130.
(92) Im, H.; Lee, S. H.; Wittenberg, N. J.; Johnson, T. W.; Lindquist, N. C.; Nagpal, P.; Norris, D. J.; Oh, S.-H. Template-Stripped Smooth Ag Nanohole Arrays with Silica Shells for Surface Plasmon Resonance Biosensing. *ACS Nano* **2011**, *5*, 6244−6253.
(93) Kim, D.; Becknell, N.; Yu, Y.; Yang, P. Room-Temperature Dynamics of Vanishing Copper Nanoparticles Supported on Silica. *Nano Lett.* **2017**, *17*, 2732−2737.
(94) Golze, S. D.; Hughes, R. A.; Rouvimov, S.; Neal, R. D.; Demille, T. B.; Neretina, S. Plasmon-Mediated Synthesis of Periodic Arrays of Gold Nanoplates using Substrate-Immobilized Seeds Lined with Planar Defects. *Nano Lett.* **2019**, *19*, 5653−5660.

https://dx.doi.org/10.1021/acs.chemmater.0c02715
Chem. Mater. 2020, 32, 6788−6799